RESEARCH ARTICLE

Thermal Cooling and System Irreversibilities of A Divergent/Convergent Channel with The Bioconvection Flow of Non-Newtonian Nanofluid

Muhammad Eisa[1], **Sohail Rehman**[2,*], **Yasir Khan**[2], **Maryam**[2] **and Gulzar Ali Khan**[2]

[1] Department of Statistics, University of Peshawar, Peshawar 25000, Khyber Pakhtunkhwa, Pakistan
[2] Department of Physical and Numerical Sciences, Qurtuba University of Science and Information Technology, Peshawar 25000, Khyber Pakhtunkhwa, Pakistan

Abstract

The laminar bioconvection flow of a nanofluid in a convergent/divergent channel is computationally analyzed. The channel features impervious, adiabatic walls. A physics-based model couples the mass, momentum, and energy conservation equations. A thermal-hydraulic and entropy production analysis is performed using the first and second laws of thermodynamics to identify ideal parameters that maximize thermal performance while minimizing system irreversibility. Fluid flow, heat-mass transfer, motile microorganism density, and system entropy are investigated as functions of the channel angle. The governing equations are reduced via scaling and solved numerically using the Keller-Box method. Results indicate that higher Reynolds numbers and cross-viscosity reduce frictional drag, while motile density decreases with the Péclet number. Heat and mass transfer rates decline with increased Brownian motion, whereas thermophoresis shows opposing effects. Nanoparticle diffusion mitigates channel overheating, aiding thermal cooling. System irreversibilities dominate in narrower sections, and entropy generation near the wall increases with thermophoresis.

Keywords: non-Newtonian fluid, converging/diverging flow, frictional drag, thermodynamic analysis, keller-Box approach, thermal cooling.

1 Introduction

Fluid flow through non-uniform cross sectional topologies such as pipe flow with different cross sectional inlet and outlet [1], blood flow through artery and vien [2], flow through converging duct [3, 4] as referred as a Jeffrey-Hamel flow. The transportation of heat within Jeffery-Hamel flows is important in both theorising and practising because it has various applications, especially in both metal and plastic sheet production technologies. From the perspective of hydrodynamics, Jeffery [22] analysed this flow for the first time in 1915, and Hamel [18] explored this subsequently in 1917. Due to their chramendous work, the flow via non-uniform morphologies was named as

Submitted: 01 December 2025
Accepted: 17 December 2025
Published: 22 December 2025

Vol. 1, **No.** 2, 2025.
10.62762/IJTSSE.2025.318713

***Corresponding author:**
Sohail Rehman
sohail@qurtuba.edu.pk

Citation
Eisa, M., Rehman, S., Khan, Y., Maryam, & Khan, G. A. (2025). Thermal Cooling and System Irreversibilities of A Divergent/Convergent Channel with The Bioconvection Flow of Non-Newtonian Nanofluid. *International Journal of Thermo-Fluid Systems and Sustainable Energy*, 1(2), 83–95.

Jeffrey-Hamel flow. The problem has exact solution in case of viscous fluid. This exact solution can be used as a benchmark for validity of Navier–Stokes equation [6]. However, due to nonlinearities of stress strain relation in case of non-Newtonian and viscoelastic models the exact solution is challenging. Thus, the numerical approach might be used to test the credibility of a rheological model (models that offer fundamental equations that connect the stress tensor to the rate of strain tensor). It is important to noted that many manufacturing and physiological liquids, such as aqueous suspended substances, polymers, sludge, fluid emulsion blood [8], etc. The analysis of Jeffery-Hamel flow is essential for investigating blood flow through arteries, nozzle flow, and its applications in biochemical and engineering sciences [23]. The Jeffery-Hamel flow within converging-diverging conduits is important for both non-Newtonian as well as Newtonian fluids and is fully addressed in literature, such as Bejan et al. [7], Banerjee et al. [5], Sheikholeslami et al. [52] and Garimella et al. [16]. Typically, a similarity transformation mechanism is employed to solve the Jeffery-Hamel flow problem, yielding a third order nonlinear differential equation. This equation is easily solved using numerical approaches, especially for the flow of non-Newtonian liquids, for which exact solutions are not always available. Several investigators have discussed the Jeffrey-Hamel flow and heat transport mechanism of viscous, NF, rheological and viscoelastic model considering different physical [11–13, 17].

The study of rheological liquids has gotten significant interest in clinical trials and other technological endeavors in recent years. The curiosity is growing because of its uses in mechanical engineering, industry, and science. It is challenging to stipulate because of its complicated nature and interactions with non-Newtonian fluids [9]. Non-Newtonian fluids are prevalent in many fields of science and engineering [19]. There is a complex connection among stress as well as deformation rate in non-Newtonian fluids [28]. This class includes various fluid models such as power law fluid, Prandtl fluid, Carreau fluid, Casson fluid, Williamson fluid, and Powell- Eyring fluid. Powell et al. [36] studied the exponentially cumulative flow on mild stress in the transport of clay, grease, and pigments. Their velocity approaching monotonically with stress at elevated stress rates. The flow mechanism under discussion in this work is the Eyring-Powell (EP) fluid. The boundary layer flow characteristic of EP fluid drives researchers in non-Newtonian fluids due to its importance in engineering and technological applications. Abegunrin et al. [1] investigated the EP fluid with a catalytic chemical reaction flowing over a parabolic sheet. They determined that the flow of fluid declared an increase in velocity. Upreti et al. [20] employed the Darcy-Forchheimer medium to examine the heat sink and source for the NF flow flowing on the elastic plate. Kumar et al. [27] established a model to analyze the flow behavior of EP fluid moving among two spinning cylinders, and the find that the EP fluid caused the upsurges in flow velocity. Salawu et al. [46] investigated the energy exploration phenomena of a EP fluid with varying thermal conductivity on a porous material. Tadesse et al. [53] examined the Darcy-Forchheimer permeability surface for the flow of ferrofluid moving over the heated stretchable surface and discovered that both inertia and porosity coefficients increase flow stability. Nazeer et al. [33] provide the computational depiction of energy estimation of EP NF moving across a flexible Riga plate. Chu et al. [13] investigated numerical solution for the flow of EP fluid across a magnetised stretchable Riga plate using the pseudo-spectral collocation approach. Nazeer et al. [34] examined the constant and variable viscosity of EP fluid while flowing through a pipe. They provide numerical and exact solution using the Keller-Box scheme and perturbation method. Jalili et al. [21] presented a non-Newtonian fluid problem and performed a thermal analysis on the stretching surface.

In thermodynamic engineering, an entropy optimization is an indicator of energy loss in any closed system. The entropy optimization method is employed for determining an extent of irreversibility. Thermal engineering equipment generate irreversibility and entropy is used as gauge to quantify the loss of energy [14]. It is employed in thermal engineering as a quantitative measure of the ultimate state irreversibility. Entropy generation in thermal engineering can help in optimizing thermal performance, evaluating improved remedies, and reducing wasted effort [24]. Using a reduction method of entropy generation, one can increase the productivity of a thermal engineering system and identify new ways to reduce the aggregate of effort that is lost. The technique was recently used in an exertion to develop NF-based thermal systems [25]. The entropy production method is used in the advance of developing standards for testing the efficiency of thermal engineering devices [26].

Bejan [7] developed the entropy generation number (Bejan Number) using second law of thermodynamics that interoperate for many challenges linked to convection. Kumar et al. [27] present a systematic assessment of entropy formation in NF flow. Shaw et al. [50] investigated the impact of shape, viscosity and interfacial cover modifications on the entropy-elevated flow of CNTs NF via a thin needle. The interface layer and morphology effects were computationally analyzed for the entropy enhanced Darcy Forchheimer electromagnetic flow of CNTs mixed with water as the base fluid to form NF in a work conducted by Nayak et al. [32]. Mandal et al. [30] investigate the entropy generation of MHD bioconvective flow of Maxwell NF comprised of gyrotactic microorganisms flowing across a radiative inclined stretchable cylinder in this study. Adesanya et al. [2] investigates the intrinsic irreversibility of the thin film flow of an incompressible viscous, pair-stress fluid down an inclined, heated conduit with an adiabatic free surface.

It is evident from the previously mentioned literature that no research has been done on the system entropy and thermal cooling of the convergent and divergent channel for the bioconvection flow of Reiner-Rivlin NF [15]. The originality of this study lies in the first-ever coupled thermal-hydraulic, entropy, and bioconvection analysis of a Reiner–Rivlin non-Newtonian NF in a converging/diverging Jeffery–Hamel channel [10], incorporating motile microorganisms, radiative heat transfer, and double-diffusion effects simultaneously. While prior works have examined NF or entropy generation in similar geometries [29], none has integrated the Reiner–Rivlin rheological model with bioconvection within a unified thermodynamic optimization framework. This research fills the gap in understanding how cross-viscosity, Brownian motion, thermophoresis, and microbial transport interact to influence thermal performance and irreversibility, providing new design insights for advanced cooling systems and bio-microfluidic devices. In order to solve the problem numerically, we apply the Keller-Box method. The results of the computations itself are presented after the argument and visual depiction of the deductions drawn from the computations. The frictional drag, heat-mass transport and entropy is reviewed in case of convergent and divergent section. It is interesting to see that the solution obtained here match the solutions seems to be reliable with experimental outcomes [31–33].

2 Problem description and fundamental flow assumptions

Consider an incompressible, time-independent and laminar flow of Reiner–Rivlin nanofluid between inclined planes. The planes are intersecting at $r = 0$ with a channel width of 2α. It is assumed that the flow originates from a source located at the junction of two planes and propagates in radial direction. Therefore, the velocity field is assumed radial $\vec{V} = v_r(r, \theta)$ with no changes in the tangential direction $v_\theta(r, \theta)$ (Figure 1).

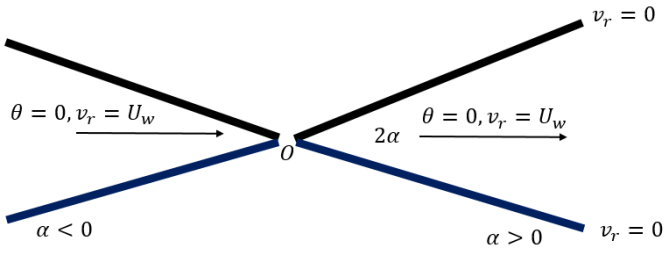

Figure 1. Illustration of the physical problem.

The presence of motile microbes within the nanofluid produces bioconvection. Since the motion of these microbes is vital in maintaining the nanoparticle floating, it is believed that the nanoparticle concentration in the base fluid will be diluted to prevent it from interfering with the mobility of the microbes. Furthermore, as Buongiorno discusses, the mobility of these nanomaterials causes two essential effects: thermophoresis and Brownian motion. As a result, the existence of these two forces is taken into account in order to achieve realistic results.

The walls of the channel are adiabatic with no slip and exhibit constant wall conditions, i.e., the fluid velocity, temperature, concentration and concentration of microorganism at the wall edges are assumed to be U_w, T_w, C_w and N_w. The base fluid is considered to be Reiner–Rivlin fluid, and the nanoparticles are immersed in the base fluid, assuming that the nanofluid remains stable, does not allow clumping in the fluid, and microbes remain alive. The floating direction of microbes is unaffected by nanoparticles. Considering that the base fluid and nanomaterials are in local thermal equilibrium, and that the velocity of the base fluid, nanoparticles, and motile microbes is the same.

3 Balance Equations

The continuity balance is governed by:

$$\mathrm{div}(\rho_f \vec{V}) = 0, \tag{1}$$

where div is the divergence operator. Here, ρ_f is the nanomaterial density and $\vec{V}$ is the corresponding flow field.

The momentum balance is governed by [34]:

$$\rho_f(\vec{V}\cdot\nabla\vec{V}) = \text{div}\,\mathbf{T}. \tag{2}$$

where $\mathbf{T}$ is the Cauchy stress tensor of Reiner–Rivlin fluid. Mathematically,

$$\mathbf{T} = -p\mathbf{I} + \boldsymbol{\sigma}_{ij}. \tag{3}$$

where $\boldsymbol{\sigma}$ is the extra stress tensor, $p\mathbf{I}$ is the undetermined part of stresses, in which p is the pressure and $\mathbf{I}$ is the unit tensor.

The mathematical expression for extra stress tensor $\boldsymbol{\sigma}_{ij}$ is defined as [35]:

$$\boldsymbol{\sigma}_{ij} = \mu_f\boldsymbol{\epsilon}_{ij} + \mu_c\boldsymbol{\epsilon}_{ik}\boldsymbol{\epsilon}_{kj}. \tag{4}$$

Here, $\boldsymbol{\epsilon}_{ij}$ is the deformation tensor, μ_f and μ_c are dynamic and cross viscosity.

In simpler notation $\boldsymbol{\sigma}_{ij}$ can be written as [36]:

$$\boldsymbol{\sigma}_{ij} = \mu_f\mathbf{A}_1 + \mu_c(\mathbf{A}_1\mathbf{A}_1), \tag{5}$$

where $\mathbf{A}_1$ is the first Rivlin–Erickson tensor.

$$\mathbf{A}_1 = \frac{1}{2}(\nabla\vec{V} + \nabla\vec{V}^T). \tag{6}$$

The balance of momentum and continuity for this flow problem take the following form [37, 38]:

$$\left(v_r\frac{\partial v_r}{\partial r}\right) = -\frac{\partial p}{\rho_f\partial r} + \frac{1}{\rho_f} \times\left(\frac{\partial}{\partial r}(T_{rr}) + \frac{1}{r}\frac{\partial}{\partial\theta}(T_{r\theta}) + \frac{T_{rr}-T_{\theta\theta}}{r}\right) = 0, \tag{7}$$

$$\left(\frac{1}{r^2}\frac{\partial}{\partial r}(r^2T_{r\theta}) + \frac{1}{r}\frac{\partial}{\partial\theta}(T_{\theta\theta})\right) = \frac{1}{\rho r}\frac{\partial p}{\partial\theta}, \tag{8}$$

$$\frac{\partial(rv_r)}{\partial r} = 0. \tag{9}$$

The components of stress tensor in notation:

$$T_{rr} = -p + \mu_f\left(2\frac{\partial v_r}{\partial r}\right) + \mu_c\left(\left(4\left(\frac{\partial v_r}{\partial r}\right)^2 + \frac{1}{r^2}\left(\frac{\partial v_r}{\partial\theta}\right)^2\right)\right) \tag{10}$$

$$T_{r\theta} = T_{\theta r} = \mu_f\left(\frac{1}{r}\frac{\partial v_r}{\partial\theta}\right) + \mu_c\left(\left(\frac{1}{r}\frac{\partial v_r}{\partial\theta}\right)\left(\frac{\partial v_r}{\partial r}\right) + \frac{2v_r}{r^2}\left(\frac{\partial v_r}{\partial\theta}\right)^2\right) \tag{11}$$

$$T_{\theta\theta} = -p + \mu_f\left(\frac{2v_r}{r}\right) + \mu_c\left(\frac{1}{r^2}\left(\frac{\partial v_r}{\partial\theta}\right)^2 + \frac{4v_r^2}{r^2}\right) \tag{12}$$

The momentum equation in the view of velocity field and components of Cauchy stress tensor takes the following form:

$$\left(v_r\frac{\partial v_r}{\partial r}\right) = -\frac{\partial p}{\rho_f\partial r} + \frac{\mu_f}{\rho_f}\left(\frac{\partial^2 v_r}{\partial r^2} + \frac{1}{r}\frac{\partial v_r}{\partial r} + \frac{1}{r^2}\frac{\partial^2 v_r}{\partial\theta^2} - \frac{v_r}{r^2}\right) + \frac{\mu_c}{\rho_f}\left[8\left(\frac{\partial v_r}{\partial r}\right)\left(\frac{\partial^2 v_r}{\partial r^2}\right) + \frac{4}{r^2}\left(\frac{\partial^2 v_r}{\partial r\partial\theta}\right)\left(\frac{\partial v_r}{\partial\theta}\right) + \frac{2}{r^2}\left(\frac{\partial^2 v_r}{\partial\theta^2}\right)\left(\frac{\partial v_r}{\partial r}\right) + \frac{2v_r}{r^3}\left(\frac{\partial^2 v_r}{\partial\theta^2}\right) - \frac{2}{r^3}\left(\frac{\partial v_r}{\partial\theta}\right)^2\right] \tag{13}$$

$$\frac{1}{\rho r}\frac{\partial p}{\partial\theta} = \frac{\mu_f}{\rho_f}\left(\left(\frac{1}{r}\frac{\partial^2 v_r}{\partial r\partial\theta}\right) - \frac{1}{r^2}\left(\frac{\partial v_r}{\partial\theta}\right)\right) + \frac{\mu_c}{\rho_f}\left(-\frac{1}{r}\left(\frac{\partial v_r}{\partial\theta}\right)\left(\frac{\partial v_r}{\partial r}\right) + \left(\frac{\partial^2 v_r}{\partial r\partial\theta}\right)\left(\frac{\partial v_r}{\partial r}\right) + \left(\frac{\partial v_r}{\partial\theta}\right)\frac{\partial^2 v_r}{\partial r^2} + \frac{2}{r}\left(\frac{\partial v_r}{\partial r}\right)\left(\frac{\partial v_r}{\partial\theta}\right)^2 - \frac{4v_r}{r^2}\left(\frac{\partial v_r}{\partial\theta}\right)^2 + \frac{4v_r}{r^2}\left(\frac{\partial v_r}{\partial\theta}\right)\left(\frac{\partial^2 v_r}{\partial\theta^2}\right) + \frac{2v_r}{r^2}\left(\frac{\partial v_r}{\partial\theta}\right)^2\right) \tag{14}$$

With corresponding Dirichlet and a von Neumann boundary condition at the central region and wall interface are governed by:

$$\begin{aligned} &v_r = U_w, \quad \frac{\partial v_r}{\partial\theta} = 0: \text{ In the middle section.}\\ &v_r = 0: \text{ Near the wall edges.} \end{aligned} \tag{15}$$

The energy equation is another name for the principle of energy balance model. A channel flow energy balance or energy conservation is represented in terms of heat transfer to or from frictional heating, radiative heat transport, double diffusion of nanomaterial and mechanical heat transfer. The energy balance for a

channel flow can be stated as follows when different heat transfer sources are considered [39, 40]:

$$(\rho c_p)_f(\vec{V}\cdot\nabla T) = \kappa_f\nabla^2 T - \nabla\cdot\mathbf{Q}_r + \boldsymbol{\sigma}_{ij}\cdot\nabla\vec{V} + (\rho c_p)_p\left(D_b(\nabla C\cdot\nabla T) + \frac{D_t}{T_\infty}(\nabla T)^2\right). \tag{16}$$

where $\mathbf{Q}_r$ is the radiative heat source. Using Rosseland approximation [41]:

$$\mathbf{Q}_r = \begin{pmatrix} q_{r,\text{rad}} = -\frac{4\sigma^*}{k^*}\frac{\partial T^4}{\partial r} \\ q_{\theta,\text{rad}} = -\frac{1}{r}\frac{4\sigma^*}{k^*}\frac{\partial T^4}{\partial \theta} \end{pmatrix}$$

where k^* and σ^* represent the absorption coefficient and Stefan–Boltzmann constant.

Using Eq. (13), and viscous dissipation term, the energy balance equation takes the following form:

$$\begin{aligned}\left(v_r\frac{\partial T}{\partial r}\right) &= \left(1+\frac{16\sigma^* T_\infty^3}{3k^*(\rho c_p)_f}\right)\left(\frac{1}{r}\frac{\partial T}{\partial r}+\frac{\partial^2 T}{\partial r^2}+\frac{1}{r^2}\frac{\partial^2 T}{\partial\theta^2}\right)\\ &+\frac{\mu_f}{(\rho c_p)_f}\left(4\left(\frac{\partial v_r}{\partial r}\right)^2+\frac{1}{r^2}\left(\frac{\partial v_r}{\partial\theta}\right)^2\right)\\ &+\frac{\mu_c}{(\rho c_p)_f}\left(4\left(\frac{\partial v_r}{\partial r}\right)^3+\frac{3}{r^2}\left(\frac{\partial v_r}{\partial\theta}\right)^2\left(\frac{\partial v_r}{\partial r}\right)\right.\\ &\left.+\frac{2v_r}{r^3}\left(\frac{\partial v_r}{\partial\theta}\right)^2\right)+\frac{(\rho c_p)_p}{(\rho c_p)_f}\left(D_b\left[\frac{\partial T}{\partial r}\frac{\partial C}{\partial r}+\frac{1}{r^2}\frac{\partial T}{\partial\theta}\frac{\partial C}{\partial\theta}\right]\right.\\ &\left.+\frac{D_t}{T_w}\left[\left(\frac{\partial T}{\partial r}\right)^2+\frac{1}{r^2}\left(\frac{\partial T}{\partial\theta}\right)^2\right]\right).\end{aligned} \tag{17}$$

In addition, equation of volumetric concentration of nanomaterial can be written as:

$$\begin{aligned}\left(v_r\frac{\partial C}{\partial r}\right) &= D_b\left(\frac{1}{r}\frac{\partial C}{\partial r}+\frac{\partial^2 C}{\partial r^2}+\frac{1}{r^2}\frac{\partial^2 C}{\partial\theta^2}\right)\\ &+\frac{D_t}{T_w}\left(\frac{1}{r}\frac{\partial T}{\partial r}+\frac{\partial^2 T}{\partial r^2}+\frac{1}{r^2}\frac{\partial^2 T}{\partial\theta^2}\right).\end{aligned} \tag{18}$$

The conservation equation for motile microorganisms is governed as [42]:

$$(\vec{V}\cdot\nabla N) = -\text{div}(bW_c\nabla N\cdot\nabla C - D_M\nabla N). \tag{19}$$

In the view of velocity field the Eq. (17) takes the form:

$$\begin{aligned}\left(v_r\frac{\partial N}{\partial r}\right) &= D_M\left(\frac{1}{r}\frac{\partial N}{\partial r}+\frac{\partial^2 N}{\partial r^2}+\frac{1}{r^2}\frac{\partial^2 N}{\partial\theta^2}\right)\\ &-\frac{bW_c}{C_w}\left(\frac{\partial N}{\partial r}\frac{\partial C}{\partial r}+\frac{1}{r^2}\frac{\partial N}{\partial\theta}\frac{\partial C}{\partial\theta}\right).\end{aligned} \tag{20}$$

Subject to the following conditions at the boundaries:

$$\frac{\partial T}{\partial\theta}=0,\quad \frac{\partial C}{\partial\theta}=0,\quad \frac{\partial N}{\partial\theta}=0 \quad \text{in the middle section.}$$

$$T=T_w,\quad C=C_w,\quad N=N_w \quad \text{near the wall edges.} \tag{21}$$

Here, D_M is microorganism diffusivity, b is the chemotaxis constant (m), W_c designates the highest speed (m/s) of swimming cells, while the product bW_c is constant, $\hat{V} = \left(\frac{bW_c}{\Delta C}\right)\nabla C$ denotes the average swimming velocity vector of the oxytactic microorganisms. D_B and D_T are the Brownian and thermophoretic diffusion coefficients. $(\rho c_p)_{\text{nf}}$ and $(\rho c_p)_p$ are the heat capacitance of nanofluid and nanoparticles, respectively.

Introducing rescaling variables [43, 44]:

$$f(\eta)=\frac{F(\theta)}{rU},\quad \eta=\frac{\theta}{\alpha},\quad \Theta=\frac{T}{T_w},\quad \psi=\frac{C}{C_w},\quad \beta=\frac{N}{N_w}. \tag{22}$$

Employing rescaling variables Eq. (20) in governing equations Eq. (10), (11), (15), (16) and (18), we have:

$$(f'''+4\alpha^2 f')+2\alpha\text{Re}\,ff'+\delta(2ff'''-4ff'-24\alpha^2 ff')=0, \tag{23}$$

$$(1+\text{Nr})\Theta''+\alpha^2\text{Pr}\,\text{Ec}\,(f'+4\alpha^2 f^2) + \text{Pr}(N_b\psi'\Theta'+N_t\Theta'^2)+\delta\text{Ec}\,(4\alpha^2 f^3-5f'^2 f)=0, \tag{24}$$

$$\psi''+\frac{N_t}{N_b}\Theta''=0, \tag{25}$$

$$\beta''-\text{Pe}\,\text{Sb}\,(\psi'\beta')=0. \tag{26}$$

Boundary conditions in dimensionless form:

$$f=1,\quad f'=0,\quad \Theta'=0,\quad \psi'=0,\quad \beta'=0\quad \text{at}\ \eta=0, \tag{27}$$

$$f=0,\quad \Theta=1,\quad \psi=1,\quad \beta=1\quad \text{at}\ \eta=1. \tag{28}$$

The modelled momentum equation reduces to the Jeffery–Hamel problem by taking $\delta = 0$, leading to [45]:

$$(f'''+4\alpha^2 f')+2\alpha\text{Re}\,ff'=0. \tag{29}$$

The dimensionless variables associated with equations:

$$\delta=\frac{\mu_c U^2}{\rho_f r},\quad \text{Re}=\frac{\alpha r U}{\nu_f},\quad \text{Pr}=\frac{\mu_f c_p}{\kappa_f},\quad \text{Ec}=\frac{U^2}{(c_p)_f(T_w-T_m)},$$

$$N_b=\frac{\epsilon D_b(C_w-C_m)}{\nu_f},\quad N_t=\frac{\epsilon D_t(T_w-T_m)}{\nu_f T_m},\quad \text{Pe}=\frac{bW_c}{C_w},\quad \text{Sb}=\frac{\nu_f}{D_M}.$$

Wall coefficients due to fluid friction, heat transport, mass transport and motile density function:

$$C_f = \frac{\sigma_{r\theta}}{\rho_f U^2}, \quad \mathrm{Nu} = -\frac{rq_w}{k_f T_w}, \\ \mathrm{Sh} = -\frac{rq_m}{D_b C_w}, \quad \mathrm{Nn} = -\frac{rq_N}{D_M N_w}. \tag{30}$$

where

$$\left.\begin{aligned} \sigma_{r\theta} &= \mu_f \left(\frac{1}{r}\frac{\partial u}{\partial \theta}\right) + \mu_c \left(\left(\frac{2}{r}\frac{\partial u}{\partial \theta}\right)\left(\frac{\partial u}{\partial r}\right) + \frac{2u}{r^2}\left(\frac{\partial u}{\partial \theta}\right)^2\right), \\ q_w &= -k_f \frac{1}{r}\left[1 + \frac{16\sigma^* T_\infty^3}{3k^*(\rho c_p)_f}\right]\left(\frac{\partial T}{\partial \theta}\right)_{\theta=\alpha}, \\ q_m &= -D_B \left(\frac{\partial C}{\partial \theta}\right)_{\theta=\alpha}, \\ q_N &= -D_M \left(\frac{\partial N}{\partial \theta}\right)_{\theta=\alpha}. \end{aligned}\right\} \tag{31}$$

The dimensionless form of physical quantities:

$$\left.\begin{aligned} C_f &= \frac{1}{\mathrm{Re}}\left(f'(1) + \lambda\left(2f(1)f^2(1) - f(1)f'(1)\right)\right), \\ \mathrm{Nu} &= -\frac{1}{\alpha}(1+\mathrm{Nr})\Theta'(1), \\ \mathrm{Sh} &= -\frac{1}{\alpha}\psi'(1), \\ \mathrm{Nn} &= -\frac{1}{\alpha}\beta'(1). \end{aligned}\right\} \tag{32}$$

4 System irreversibilities (Entropy generation)

The energy loss mechanism within channel is measured using second law of thermodynamic. Here, the system irreversibilities arises due to frictional heating between channel surface and fluid contact, heat loss due to conduction, energy loss due to cooling mechanism of nanomaterial diffusion and motile microorganism.

The total volumetric entropy is the sum of energy transport, frictional heating and mass transport is governed by the following mathematical relation [2, 46, 47]:

$$\begin{aligned} N_{\mathrm{gen}} =& \frac{k_f}{T_0^2}\left(1 + \frac{16\sigma^* T_\infty^3}{3k^*(\rho c_p)_f}\right)\left(\frac{1}{r}\frac{\partial T}{\partial r} + \frac{\partial^2 T}{\partial r^2} + \frac{1}{r^2}\frac{\partial^2 T}{\partial \theta^2}\right) \\ &+ \frac{1}{T_0}\left(\mu_f\left(4\left(\frac{\partial v_r}{\partial r}\right)^2 + \frac{1}{r^2}\left(\frac{\partial v_r}{\partial \theta}\right)^2\right)\right. \\ &\left. + \frac{\mu_c}{(\rho c_p)_f}\left(4\left(\frac{\partial v_r}{\partial r}\right)^3 + \frac{3}{r^2}\left(\frac{\partial v_r}{\partial \theta}\right)^2\left(\frac{\partial v_r}{\partial r}\right) + \frac{2v_r}{r^3}\left(\frac{\partial v_r}{\partial \theta}\right)^2\right)\right) \\ &+ \frac{RD_B}{T_0}\left(\frac{\partial T}{\partial r}\frac{\partial C}{\partial r} + \frac{1}{r^2}\frac{\partial T}{\partial \theta}\frac{\partial C}{\partial \theta}\right) + \frac{RD_B}{C_0}\left(\left(\frac{\partial C}{\partial r}\right)^2 + \frac{1}{r^2}\left(\frac{\partial C}{\partial \theta}\right)^2\right) \\ &+ \frac{RD_M}{T_0}\left(\frac{\partial T}{\partial r}\frac{\partial N}{\partial r} + \frac{1}{r^2}\frac{\partial T}{\partial \theta}\frac{\partial N}{\partial \theta}\right) + \frac{RD_M}{C_0}\left(\left(\frac{\partial N}{\partial r}\right)^2 + \frac{1}{r^2}\left(\frac{\partial N}{\partial \theta}\right)^2\right). \end{aligned} \tag{33}$$

The total entropy generation can be decomposed as:

$$N_{T,\mathrm{gen}} = N_{H,\mathrm{gen}} + N_{V,\mathrm{gen}} + N_{M,\mathrm{gen}}. \tag{34}$$

In view of dimensionless variables, we have:

$$\begin{aligned} N_G =& \frac{r^2\alpha^2 N_{T,\mathrm{gen}}}{k_f} \\ =& \alpha^2(1+\mathrm{Nr})\Theta'^2(\eta) + \mathrm{Br}\left((f' + 4\alpha^2 f^2)\right. \\ &\left. + \delta(4\alpha^2 f^3 - 5f'^2 f)\right) + L_1(\psi'\Theta' + \Theta'^2) \\ &+ L_2(\psi'\beta' + \beta'^2), \end{aligned} \tag{35}$$

where

$$\mathrm{Br} = \mathrm{Pr}\,\mathrm{Ec}, \quad C_0 = \frac{C + C_W}{2}, \quad T_0 = \frac{T + T_W}{2}, \\ L_1 = \frac{RD_B C_W}{k_f}, \quad L_2 = \frac{RD_M N_W}{k_f}. \tag{36}$$

5 Numerical solution using Keller-box (finite-difference technique)

The equations under consideration are streamlined into a set of coupled, non-linear differential equations with suitable boundary conditions after applying the similarity modification to the governing equations and the boundary conditions. Finally, the Keller-Box technique is used to solve the system of similarity equations with boundary conditions [48]. With variable spacing, this approach is reliable and has second order precision. The converted differential equations and boundary conditions are expressed in terms of a first order system, which is then changed to a set of finite difference equations using central differences. The non-linear algebraic expressions are streamlined using Newton's method, and the consequent linear system of equations is solved using the block tri-diagonal elimination procedure. For the sake of brevity, the numerical solution process is not described in detail here. The detail solution scheme can

be found in the following recent studies [49–51]. It is worth noting that a uniform grid of $\Delta\eta$=0.01 provides adequate accuracy with an error tolerance of less than 10^{-6}. To validate the current findings, the results are compared with Verma et al. [54] and Sari et al. [47] as depicted in Table 1. We have an outstanding alliance with the standards that are already recognized. By using the Keller Box approach, this result provides certainty of our current computations.

6 Results and discussion

In this study, the system entropy and channel cooling mechanism have been investigated together with several other physical quantities, comprising with gyrotactic organisms. The Buongiorno model has been introduced to the mathematical equations, which take Brownian movement and the thermophoresis of nanoparticles in fluid into account. The statistical outcomes are scrutinized to obtain understanding of the physical phenomena that occur inside the system and to comprehend the presence of significant limits on fluid flow, mass, heat, and motile microbe transmission in order to improve the thermal efficacy of the oblique channel.

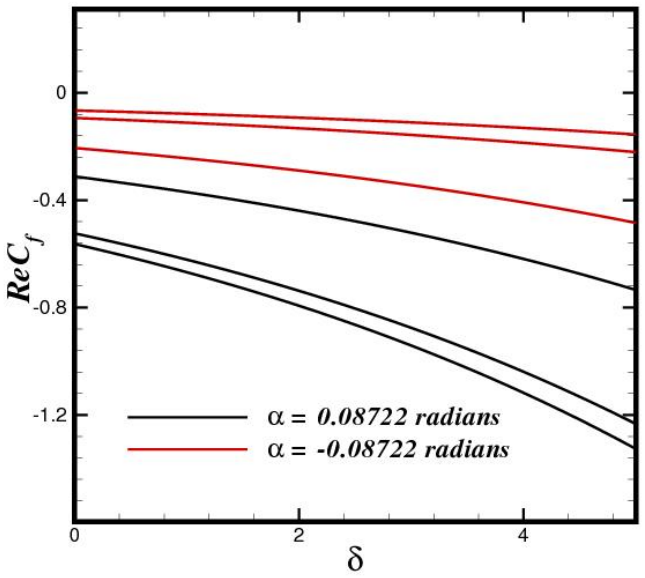

Figure 2. Visualization of frictional coefficient within oblique portion of the channel against fluid parameter η keeping fixed channel width and Re=50.

The effects of manipulating factors such as cross viscosity parameter δ and Reynold number Re on frictional coefficient of a non-Newtonian fluid along a convergent and diverging section are anticipated

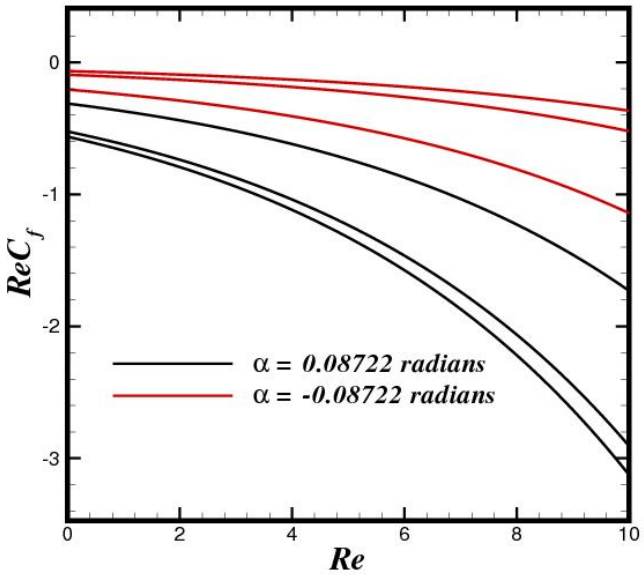

Figure 3. Visualization of frictional coefficient within oblique portion of the channel against inertial parameter Re keeping fixed channel width η=0.5.

in Figures 2 and 3, respectively. Skin friction is the frictional drag applied by the liquid on the interface of the channel. It quantifies the impedance to fluid mobility along the surface. Tangential skin friction is the frictional drag operating in the track of the flow comparable to the channel wall. The cross viscosity parameter is important in both circumstances for lowering skin friction. Higher Reiner-Rivlin parameter values increase liquid viscosity and obstruction to flow, lowering the skin friction. The Reiner-Rivlin parameter controls the flow performance and viscosity of the liquid, which helps to reduce the apparent frictional force. From both section it is evident that the effect of frictional coefficient is higher for convergent (narrower) section. Physically, the narrower section produces additional force, which shrink the fluid into a narrower exit. Thus, as a result of additional drag within the flow regime and surface contact the frictional coefficient decrease. It is well known that as the Reynolds number grows, the Newtonian fluid flow velocity profile in a diverging channel appears narrower [54]. It is inferred that the Reynolds number may alter the flow; in other words, as the Reynolds number increases, the mathematical sign of the velocity gradient at the wall tends to fluctuate, resulting in the separation phenomena. In a converging channel, on the other hand, when the Reynolds number grows, the fluid constituents accelerate [55]. The area of the velocity gradient near

Table 1. Comparison of velocity profile $f(\eta)$ with existing studies.

$\eta = \frac{\theta}{\alpha}$	$f(\eta)$			Error (%)
	Verma et al. [54]	Sari et al. [47]	Present study	
-1.0	0.00000000	0.00000000	0.000000	0.000000
-0.75	0.515827995	0.515364034	0.515357	0.000463
-0.50	0.811457376	0.811498203	0.811467	0.000004
-0.25	0.956861924	0.956869209	0.956867	0.000004
0.00	1.00000000	1.00000000	1.000000	0.000000
0.25	0.956861924	0.956869209	0.956868	0.000009
0.50	0.811457376	0.811098203	0.811098	0.000000
0.75	0.515827995	0.515364034	0.515378	0.000006
1.0	0.00000000	0.00000000	0.000000	0.000000

the wall grows as the Reynolds number increases, as seen. As an outcome, increasing the channel half-angle may cause the splitting behavior to occur in a diverging channel since it reduces the velocity gradient near the wall. In contrast, in a converging channel, the channel half-angle accelerates the fluid elements and raises the velocity gradient near the wall.

The Nusselt number Nu is a dimensionless physical quantity used to calculate the rate of energy transport in a fluid system. It offers a quantity of energy transport efficiency. In both circumstances, the Nu drops as the thermophoresis and Brownian motion parameters N_b increase (Figure 4(a, b) and Figure 5(a, b)). In the convergent section, growing the N_b results in increased accumulation of nanomaterials at the interface. This aggregation enhances the energy transport from the liquid to the nanomaterials while decreasing convective energy transport rate and yielding a inferior Nu.

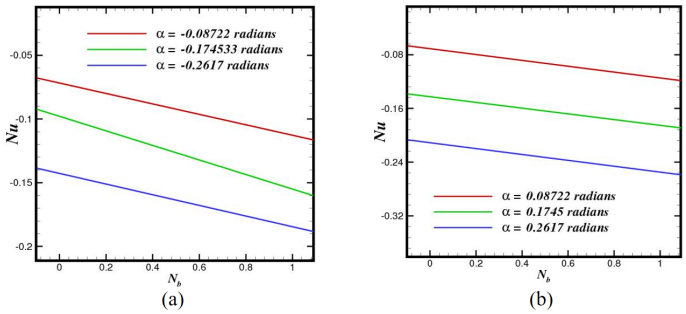

Figure 4. Visualization of energy transport coefficient within oblique portion of the channel (a) convergent (b) divergent against Brownian parameter N_b keeping fixed channel width and N_t=0.4, Pr=6.2, Ec=0.1, Nr=0.5, δ=0.5.

An upsurge in Brownian motion enhances nanoparticle dispersion throughout the fluid. The scattering lowers the volumetric concentration of nanomaterials near the interface, resulting in less energy transport rate from liquid to nanomaterials. When Brownian motion increases, the convective heat transmission and the Nu decrease. The discrepancy is caused by a variance in thermal slopes in the flow track. The temperature increases in the flow direction in the convergent situation, generating advantageous situations for convective energy transport rate and resulting in a greater Nu. Along the divergent scenario, the thermal profile drops along the flow direction, resulting in less convective heat transfer and a inferior Nu.

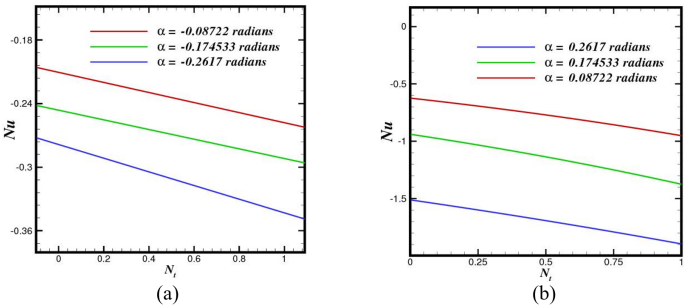

Figure 5. Visualization of energy transport coefficient within oblique portion of the channel (a) convergent (b) divergent against thermophoresis parameter N_t keeping fixed channel width and N_b=0.4, Pr=6.2, Ec=0.1, Nr=0.5, δ=0.5.

The thermophoretic factor simulates the mobility of nanomaterials in a liquid due to a temperature gradient. Strengthening the thermophoretic variable improves nanoparticle mobility and formation adjacent the wall. As a result, additional energy is transported from the nanomaterials to the liquid, enhancing convective energy transport rate as a result the Nu decreases. Brownian motion is the random movement of nanomaterials caused by temperature instabilities. In the case of divergent section, greater Brownian motion causes enhanced scattering and diffusion of nanomaterials across the fluid. This scattering diminishes the volumetric concentration of nanomaterials near the surface, resulting in less

heat transfer from the nanoparticles to the fluid. As a result of increasing Brownian motion, convective heat transmission and Nu drop. Thus, the use of Brownian and thermophoretic variable can be used for channel cooling.

The Sherwood number Sh is a dimensionless physical quantity that describes the rate of mass transport rate in a fluid system. It serves as an indicator of transference of mass efficiency. A higher Sh suggests improved mass transport rate efficiency and convective mass transport rate. The internal temperature of the fluid near the surface rises in the convergent channel instance, producing a positive environment for mass transfer. Higher heat promote the diffusion of nanomaterials from the fluid, resulting in enhanced mass transport rate and a larger Sh.

In the diverging scenario, the thermal profile near the wall declined in the flow track. Because of the effect of the thermal gradient on the concentration slope of nanomaterials, mass transport from the wall to the fluid is diminished. As a result, the Sherwood number is lower in the case of divergent channel flow than in the case of convergent channel flow.

The Sh quantity reduces as N_b improve and increases as N_t increase (Figure 6 and Figure 7). Higher N_b result in higher surface temperatures, which reduces the concentration gradient and, as a result, the lower mass transfer rate. As the N_b is increased, the Sh falls. The N_b takes into consideration the random movement of nanomaterials caused by thermal variations. Increasing the N_b improves the nanomaterials dispersion throughout the fluid, reducing their concentration near the surface. As the concentration of nanoparticles declines, the mass transport rate reduces, resulting in a decreased Sh.

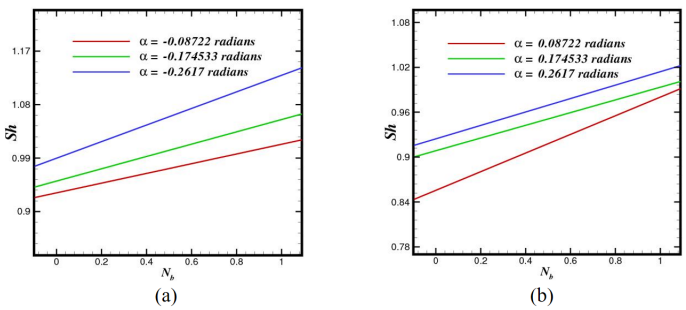

Figure 6. Visualization of mass transport coefficient within oblique portion of the channel (a) convergent (b) divergent against Brownian parameter N_b keeping fixed channel width and N_t=0.4, Pr=6.2, Ec=0.1, Nr=0.5, δ=0.5.

The thermophoresis parameter represents

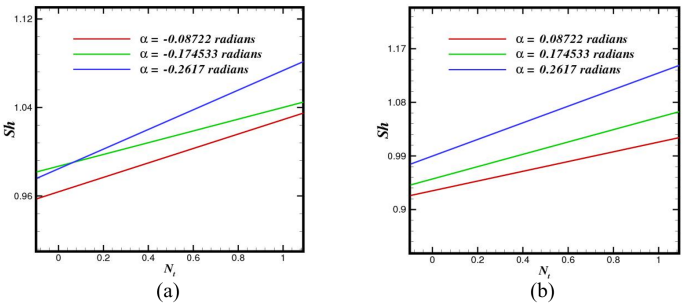

Figure 7. Visualization of energy transport coefficient within oblique portion of the channel (a) convergent (b) divergent against thermophoresis parameter N_t keeping fixed channel width and N_b=0.4, Pr=6.2, Ec=0.1, Nr=0.5, δ=0.5.

nanoparticle mobility caused by a temperature differential. By increasing the N_t, nanoparticles are deposited at the surface, improving their contact and mass transfer with the fluid. Thus, as the thermophoresis parameter increases, the Sh increases in both section.

The dimensionless microorganism transfer rate, also known as the transformed density of microorganisms, is a measure used to compute the transmission of microorganisms in a fluid system. It quantifies the density of microorganisms or concentration in a fluid system. It allows for the judgement and investigation of microbe performance across any systems, as well as insights on their transit and distribution. Higher temperatures near the surface facilitate the development and movement of microorganisms in the diverging instance. The increasing temperature gradient improves fluid motion and nutrient transfer, allowing microorganisms to move and accumulate, resulting in a larger motile density number. In contrast, the thermal field at the wall drops in the flow direction in the case of a converging channel. This temperature gradient influences microbe mobility and transport, possibly controlling their evolution and motion. The gradients of temperature are less favorable for microorganisms than concentration gradients, resulting in a minor motile density number. Growing Peclet number values Pe reduces the density profile of motile microorganisms (Figure 8). The aforementioned physical parameter behavior is caused by the fact that as microbe diffusivity decreases, the microorganism's speed also decreases.

The degree of entropy required for irreversible operations is referred to as entropy creation. According to Figure 9, larger N_b decreases the entropy production N_G in the channel middle while increasing it further

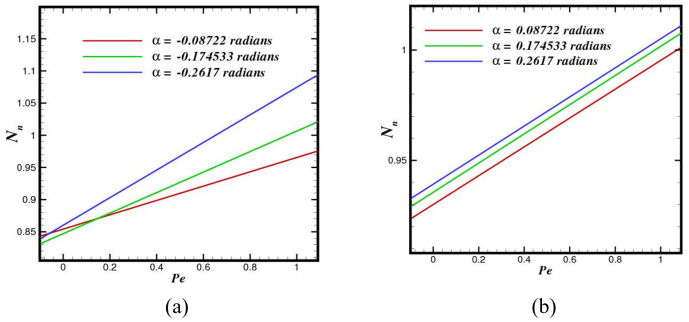

Figure 8. Visualization of motile density within oblique portion of the channel (a) convergent (b) divergent against Peclet number Pe keeping fixed channel width and N_t=0.4, Pr=6.2, Ec=0.1, Nr=0.5, δ=0.5, Sb=0.5.

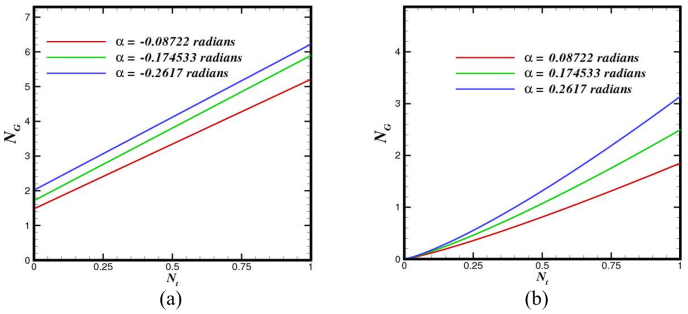

Figure 10. Visualization of entropy within oblique portion of the channel (a) convergent (b) divergent against thermophoresis parameter N_t keeping fixed channel width and L_1=0.4, Pr=6.2, Ec=0.1, Nr=0.5, δ=0.5, L_2=0.5.

away from the wall. The rise in N_b promotes Brownian motion of nanoparticles. As a result, energy is transferred to the far flow region, and the kinetic energy of nanoparticles is enhanced. As a result, entropy formation occurs distant from the walls.

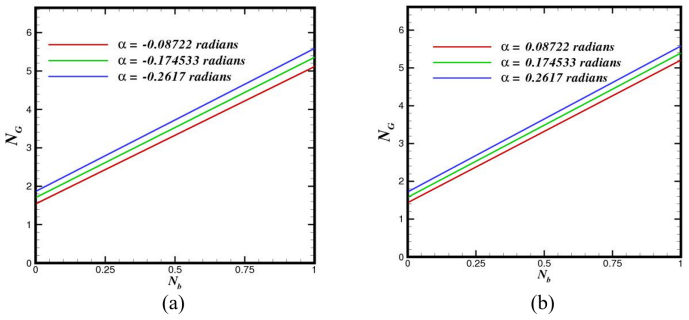

Figure 9. Visualization of entropy within oblique portion of the channel (a) convergent (b) divergent against Brownian parameter N_b keeping fixed channel width L_1=0.4, Pr=6.2, Ec=0.1, Nr=0.5, δ=0.5, L_2=0.5.

When N_b is increased near the walls, the frictional heating effect becomes more powerful in comparison to the irreversibility of energy transfer. After a certain distance, the energy transmission becomes more efficient for escalating N_b. The nanoliquid cannot freely infiltrate due to its low permeability and high fluid confrontation. The conduction mechanism of heat transfer was applied in this case. The thermophoretic force endures to generate entropy far away from the wall of the channel by raising N_t (Figure 10). By amplifying the impact of thermophoretic diffusion, the viscous effect outperforms the energy transport rate affects closer to the wall. Away from the center, however, the rising N_t is dominated by the energy transfer influence, which disables the frictional heating effect, resulting in an increase in N_G.

7 Conclusion

The flow of Reiner-Rivlin NF through convergent and divergent channels in the presence of gyrotactic organisms is the focus of this research. Various impacts such as heat radiation and double diffusion of nanomaterials are also considered. The system of conventional differential equations is solved computationally using Keller-Box method. The objective of this article is to figure out the various factors impact on thermal cooling and system entropy. The frictional coefficient, Sherwood, local Nusselt, and the density numbers are evaluated. The computational findings are offered visually, allowing for graphical investigation of parameter effects. The study yields several notable conclusions, both for convergent and divergent channel sections:

- The Reiner-Rivlin parameter controls the flow performance and cross viscosity of the liquid, which helps to reduce the system frictional coeffeicent. Nearly similar trend was seen for Reynold number.
- The frictional coefficient is higher in case of convergent section. The narrower section produce additional drag between the fluid flow and wall contact.
- Increasing the Brownian motion, the convective heat transmission and the Nusselt number decreases.
- Strengthening the thermophoretic variable improves the nanoparticle mobility and more heat is transferred to the surface causing in decrease in energy transport rate.
- The Brownian and thermophoretic variable are favorable for thermal cooling and can be used as remote control to adjust the channel overheating.

- The action of Brownian and thermophoretic variable against mass transport is opposite.
- Growing Peclet number values Pe reduces the density profile of motile microorganisms.
- Elevated thermal profile near the surface facilitate the development and movement of microorganisms in the diverging instance.
- Large values of N_b the entropy production N_G in the channel middle decreases, while increasing it further away from the wall.
- Rising the thermophoretic diffusion is dominated by the energy transfer impact, which overcomes the frictional heating effect, resulting in an increase in N_G.

Future research could employ experimental environments with synthetic NF and motile microorganisms in scaled converging-diverging channels for testing the computational results. The model practical relevance in advanced thermal management and bio-microfluidic systems would be further improved by expanding it to three-dimensional, transient, or turbulent flows, adding temperature-dependent features, and investigating hybrid NF or magnetic field effects.

Data Availability Statement

Data will be made available on request.

Funding

This work was supported without any funding.

Conflicts of Interest

The authors declare no conflicts of interest.

Ethical Approval and Consent to Participate

Not applicable.

References

[1] Abegunrin, O. A., Animasaun, I. L., & Sandeep, N. (2018). Insight into the boundary layer flow of non-Newtonian Eyring-Powell fluid due to catalytic surface reaction on an upper horizontal surface of a paraboloid of revolution. *Alexandria Engineering Journal, 57*(3), 2051–2060. [CrossRef]

[2] Adesanya, S. O., & Makinde, O. D. (2015). Irreversibility analysis in a couple stress film flow along an inclined heated plate with adiabatic free surface. *Physica A: Statistical Mechanics and its Applications, 432*, 222–229. [CrossRef]

[3] Puneeth, V., Narayan, S. S., Manjunatha, S., & Makinde, O. D. (2022). Numerical simulation of Jeffrey–Hamel flow of nanofluid in the presence of gyrotactic microorganisms. *International Journal of Ambient Energy, 43*(1), 6095-6107. [CrossRef]

[4] Avramenko, A. A., Kovetska, Y. Y., & Shevchuk, I. V. (2023). Lorenz approach for analysis of bioconvection instability of gyrotactic motile microorganisms. *Chaos, Solitons & Fractals, 166*, 112957. [CrossRef]

[5] Banerjee, A., Mahato, S. K., Bhattacharyya, K., & Chamkha, A. J. (2021). Divergent channel flow of Casson fluid and heat transfer with suction/blowing and viscous dissipation: Existence of boundary layer. *Partial Differential Equations in Applied Mathematics, 4*, 100172. [CrossRef]

[6] Barzegar Gerdroodbary, M., Rahimi Takami, M., & Ganji, D. D. (2015). Investigation of thermal radiation on traditional Jeffery–Hamel flow to stretchable convergent/divergent channels. *Case Studies in Thermal Engineering, 6*, 28–39. [CrossRef]

[7] Bejan, A. (1979). A Study of Entropy Generation in Fundamental Convective Heat Transfer. *Journal of Heat Transfer, 101*(4), 718–725. [CrossRef]

[8] Boudjemline, A., Ahmad, I., Rehman, S., Hashim, & Khedher, N. B. (2023). Jeffery-Hamel flow extension and thermal analysis of Oldroyd-B NF in expanding channel. *Journal of Non-Equilibrium Thermodynamics, 48*(1), 75–90. [CrossRef]

[9] Boujelbene, M., Rehman, S., Alqahtani, S., & Alshehery, S. (2023). Second law assessment of injected nanoparticles to blood flow with thermal radiation and magnetic field in conduit artery. *Journal of the Taiwan Institute of Chemical Engineers, 150*, 105074. [CrossRef]

[10] Arain, M. B., Bhatti, M. M., Zeeshan, A., & Alzahrani, F. S. (2021). Bioconvection Reiner-Rivlin nanofluid flow between rotating circular plates with induced magnetic effects, activation energy and squeezing phenomena. *Mathematics, 9*(17), 2139. [CrossRef]

[11] Bouzidi, M., Maleki, H., Ambreen, T., Gholami, M., Tlili, I., & Khan, M. I. (2025). Exploring Darcy-Brinkman model and magnetic dipole impact on heat and mass transfer of Stefan blowing slip flow of ferromagnetic Prandtl NF. *Case Studies in Thermal Engineering, 75*, 106999. [CrossRef]

[12] Cebeci, T., & Bradshaw, P. (2012). *Physical and Computational Aspects of Convective Heat Transfer*. Springer Science & Business Media.

[13] Chu, Y. M., Ahmad, F., Khan, M. I., Nazeer, M., Hussain, F., Khan, N. B., ... & Mei, L. (2021). Numerical and scale analysis of non-Newtonian fluid (Eyring-Powell) through pseudo-spectral collocation method (PSCM) towards a magnetized stretchable Riga surface. *Alexandria Engineering Journal, 60*(2),

2127-2137. [CrossRef]

[14] Sparrow, E. M., Abraham, J. P., & Minkowycz, W. J. (2009). Flow separation in a diverging conical duct: Effect of Reynolds number and divergence angle. *International Journal of Heat and Mass Transfer, 52*(13-14), 3079-3083. [CrossRef]

[15] Gamaoun, F., Ullah, Z., Ahammad, N. A., Fadhl, B. M., Makhdoum, B. M., & Khan, A. A. (2023). Effects of thermal radiation and variable density of NF heat transfer along a stretching sheet by using Keller Box approach under magnetic field. *Thermal Science and Engineering Progress, 41*, 101815. [CrossRef]

[16] Garimella, S. M., Anand, M., & Rajagopal, K. R. (2022). Jeffery–Hamel flow of a shear-thinning fluid that mimics the response of viscoplastic materials. *International Journal of Non-Linear Mechanics, 144*, 104084. [CrossRef]

[17] Haines, P. E., Hewitt, R. E., & Hazel, A. L. (2011). The Jeffery–Hamel similarity solution and its relation to flow in a diverging channel. *Journal of Fluid Mechanics, 687*, 404–430. [CrossRef]

[18] Hamel, G. (1917). Spiralförmige Bewegungen zäher Flüssigkeiten. *Jahresbericht der Deutschen Mathematiker-Vereinigung, 25*, 34–60.

[19] Harley, C., Momoniat, E., & Rajagopal, K. R. (2018). Reversal of flow of a non-Newtonian fluid in an expanding channel. *International Journal of Non-Linear Mechanics, 101*, 44–55. [CrossRef]

[20] Upreti, H., Pandey, A. K., Kumar, M., & Makinde, O. D. (2020). Ohmic heating and non-uniform heat source/sink roles on 3D Darcy–Forchheimer flow of CNTs nanofluids over a stretching surface. *Arabian Journal for Science and Engineering, 45*(9), 7705-7717. [CrossRef]

[21] Jalili, B., Ganji, A. D., Jalili, P., Salman Nourazar, S., & Ganji, D. D. (2022). Thermal analysis of Williamson fluid flow with Lorentz force on the stretching plate. *Case Studies in Thermal Engineering, 39*, 102374. [CrossRef]

[22] Jeffery, G. B. (1915). L. The two-dimensional steady motion of a viscous fluid. *The London, Edinburgh, and Dublin philosophical magazine and journal of science, 29*(172), 455-465. [CrossRef]

[23] Jotkar, M. R., & Govindarajan, R. (2017). Non-modal stability of Jeffery-Hamel flow. *Physics of Fluids, 29*(6), 064107. [CrossRef]

[24] Khan, S. A., Hayat, T., & Alsaedi, A. (2023). Bioconvection entropy optimized flow of Reiner-Rivlin nanoliquid with motile microorganisms. *Alexandria Engineering Journal, 79*, 81–92. [CrossRef]

[25] Khan, U., Sikandar, W., Ahmed, N., & Mohyud-Din, S. T. (2016). Effects of Velocity Slip on MHD Flow of a Non-Newtonian Fluid in Converging and Diverging Channels. *International Journal of Applied and Computational Mathematics, 2*(4), 469–483. [CrossRef]

[26] Torabi, M., Zhang, K., Karimi, N., & Peterson, G. P. (2016). Entropy generation in thermal systems with solid structures–a concise review. *International Journal of Heat and Mass Transfer, 97*, 917-931. [CrossRef]

[27] Kumar, D., Ramesh, K., & Chandok, S. (2020). Mathematical modeling and simulation for the flow of magneto-Powell-Eyring fluid in an annulus with concentric rotating cylinders. *Chinese Journal of Physics, 65*, 187–197. [CrossRef]

[28] Mahian, O., Kianifar, A., Sahin, A. Z., & Wongwises, S. (2014). Entropy generation during Al2O3/water NF flow in a solar collector: Effects of tube roughness, nanoparticle size, and different thermophysical models. *International Journal of Heat and Mass Transfer, 78*, 64–75. [CrossRef]

[29] Mahian, O., Mahmud, S., & Heris, S. Z. (2012). Effect of Uncertainties in Physical Properties on Entropy Generation Between Two Rotating Cylinders With NF. *Journal of Heat Transfer, 134*(10), 101704. [CrossRef]

[30] Mandal, S., Shit, G. C., Shaw, S., & Makinde, O. D. (2022). Entropy analysis of thermo-solutal stratification of NF flow containing gyrotactic microorganisms over an inclined radiative stretching cylinder. *Thermal Science and Engineering Progress, 34*, 101379. [CrossRef]

[31] Mustafa, M., Ahmad Khan, J., Hayat, T., & Alsaedi, A. (2015). Analytical and numerical solutions for axisymmetric flow of NF due to non-linearly stretching sheet. *International Journal of Non-Linear Mechanics, 71*, 22–29. [CrossRef]

[32] Nayak, M. K., Shaw, S., Ijaz Khan, M., Makinde, O. D., Chu, Y.-M., & Khan, S. U. (2021). Interfacial layer and shape effects of modified Hamilton's Crosser model in entropy optimized Darcy-Forchheimer flow. *Alexandria Engineering Journal, 60*(4), 4067–4083. [CrossRef]

[33] Nazeer, M., Khan, M. I., Rafiq, M. U., & Khan, N. B. (2020). Numerical and scale analysis of Eyring-Powell NF towards a magnetized stretched Riga surface with entropy generation and internal resistance. *International Communications in Heat and Mass Transfer, 119*, 104968. [CrossRef]

[34] Nazeer, M., Hussain, F., Khan, M. I., Kadry, S., Chu, Y.-M., & Khan, S. U. (2019). Effects of Constant and Space-Dependent Viscosity on Eyring–Powell Fluid in a Pipe: Comparison of the Perturbation and Explicit Finite Difference Methods. *Zeitschrift für Naturforschung A, 74*(11), 961–969. [CrossRef]

[35] Ojiambo, V., Kinyanjui, M., & Kimathi, M. (2018). A study of two-phase Jeffery Hamel flow in a geothermal pipe.

[36] Powell, R. E., & Eyring, H. (1944). Mechanisms for the Relaxation Theory of Viscosity. *Nature, 154*(3909), 427–428. [CrossRef]

[37] Ullah, K., Fiza, M., Ullah, H., Jan, A. U., Akgül, A., Hendy, A., ... & Khan, I. (2025). Deep learning

investigation of ternary hybrid nanofluid flow with nonlinear heat source-sink and Cattaneo-Christov heat flux model with Joule effect. *Proceedings of the Institution of Mechanical Engineers, Part N: Journal of Nanomaterials, Nanoengineering and Nanosystems*, 23977914251343344. [CrossRef]

[38] Rehman, S., & NASR, S. (2025). Optimization of MHD Jeffrey-Hamel flow in convergent–divergent channels with slip and viscous-dissipation: vorticity–stream-function analysis of flow reversal and heat transfer. *Journal of Taibah University for Science, 19*(1), 2548630. [CrossRef]

[39] Rehman, S., Almubaddel, F. S., Mahrous, Y. M., Alsadoun, F. A., Abouzied, A. S., & Hashim. (2023). A generalization of Jeffrey-Hamel problem to Reiner-Rivlin model for energy and thermodynamic analysis using Keller-Box computational framework. *Case Studies in Thermal Engineering, 50*, 103462. [CrossRef]

[40] Rehman, S., Alqahtani, S., Hashim, & Alshehery, S. (2023). On the thermal performance during flow dynamics of viscoelastic fluid in a channel: Jaffrey–Hamel extension. *Neural Computing and Applications, 35*(29), 21949–21965. [CrossRef]

[41] Rehman, S., Hashim, Alqahtani, S., Hadj Hassine, S. B., & Eldin, S. M. (2023). Thermohydraulic and irreversibility assessment of Power-law fluid flow within wedge shape channel. *Arabian Journal of Chemistry, 16*(3), 104475. [CrossRef]

[42] Rehman, S., Al-Yarimi, F. A., Alqahtani, S., & Awad, M. (2023). Dissipative flow features of Carreau nanofluid with thermal radiation inside plane wall channel: Jeffery-Hamel analysis. *Propulsion and Power Research, 12*(2), 253-272. [CrossRef]

[43] Sadeghy, K., Khabazi, N., & Taghavi, S.-M. (2007). Magnetohydrodynamic (MHD) flows of viscoelastic fluids in converging/diverging channels. *International Journal of Engineering Science, 45*(11), 923–938. [CrossRef]

[44] Sahoo, B., & Shevchuk, I. V. (2019). Heat transfer due to revolving flow of Reiner-Rivlin fluid over a stretchable surface. *Thermal Science and Engineering Progress, 10*, 327–336. [CrossRef]

[45] Salahuddin, T. (2020). Carreau fluid model towards a stretching cylinder: Using Keller box and shooting method. *Ain Shams Engineering Journal, 11*(2), 495–500. [CrossRef]

[46] Salawu, S. O., Kareem, R. A., & Shonola, S. A. (2019). Radiative thermal criticality and entropy generation of hydromagnetic reactive Powell–Eyring fluid in saturated porous media with variable conductivity. *Energy Reports, 5*, 480–488. [CrossRef]

[47] Sari, M. R., Kezzar, M., & Adjabi, R. (2016). Heat transfer of copper/water NF flow through converging-diverging channel. *Journal of Central South University, 23*(2), 484–496. [CrossRef]

[48] Shah, S. O., Rehman, S., Osman, M., Afridi, S., Ben Hadj Hassine, S., & Ullah, U. (2024). Optimum thermal design for heat and mass transfer of non-Newtonian liquid within converging conduit with thermal jump and zero-mass flux. *Case Studies in Thermal Engineering, 53*, 103817. [CrossRef]

[49] Shukla, N., Rana, P., & Pop, I. (2020). Second law thermodynamic analysis of thermo-magnetic Jeffery–Hamel dissipative radiative hybrid nanofluid slip flow: existence of multiple solutions. *The European Physical Journal Plus, 135*(10), 1-24. [CrossRef]

[50] Shaw, S., Patra, A., Misra, A., & Nayak, M. K. (2022). Assisting/opposing/forced convection flow on entropy-optimized MHD NF with variable viscosity: Interfacial layer and shape effects. *Heat Transfer, 51*(1), 578–603. [CrossRef]

[51] Shaw, S., Shit, G. C., & Tripathi, D. (2022). Impact of drug carrier shape, size, porosity and blood rheology on magnetic nanoparticle-based drug delivery in a microvessel. *Colloids and Surfaces A: Physicochemical and Engineering Aspects, 639*, 128370. [CrossRef]

[52] Sheikholeslami, M., Ganji, D. D., Ashorynejad, H. R., & Rokni, H. B. (2012). Analytical investigation of Jeffery-Hamel flow with high magnetic field and nanoparticle by Adomian decomposition method. *Applied Mathematics and Mechanics (English Edition), 33*(1), 25–36. [CrossRef]

[53] Tadesse, F. B., Makinde, O. D., & Enyadene, L. G. (2021). Hydromagnetic stagnation point flow of a magnetite ferrofluid past a convectively heated permeable stretching/shrinking sheet in a Darcy–Forchheimer porous medium. *Sādhanā, 46*(3), 115. [CrossRef]

[54] Verma, L., Meher, R., Hammouch, Z., & Baskonus, H. M. (2022). Effect of heat transfer on hybrid nanofluid flow in converging/diverging channel using fuzzy volume fraction. *Scientific Reports, 12*(1), 20845. [CrossRef]

[55] Usman Rashid, M., & Mustafa, M. (2021). A study of heat transfer and entropy generation in von Kármán flow of Reiner-Rivlin fluid due to a stretchable disk. *Ain Shams Engineering Journal, 12*(1), 875–883. [CrossRef]

Dr. Sohail Rehman is an Assistant Professor at Qurtuba University Peshawar, Pakistan. He holds a Ph.D. in Applied Mathematics from Islamia College Peshawar. His research focuses on non-Newtonian fluid dynamics and heat/mass transfer, with expertise in Jeffrey-Hamel flow, MHD, entropy generation, and nanofluid bioconvection, published in multiple international journals. (Email: sohail08ktk@gmail.com)